DETECTION OF IN-PLANE ORBITAL MANOEUVRES FROM A CATALOGUE OF GEOSTATIONARY OBJECTS

Phuong Linh Ngo and Carlos Yanez

Centre National D'Etudes Spatiales (CNES), 18 Avenue Edouard Belin, 31401 Toulouse, France

ABSTRACT

This study is focused on the detection of orbital in-plane manoeuvres from historical orbit data contained in a catalogue of space objects. The proposed method is developed specifically for objects on the geostationary orbit (GEO) with the primary objective of detecting station keeping (SK) manoeuvres. Thereby, the longitudinal motion and the evolution of the eccentricity vector of a spacecraft is first analysed. These orbital parameters are affected by in-plane manoeuvres. If a spacecraft does not execute a manoeuvre thrust, its motion will only be affected by natural perturbation forces. Accordingly, the longitudinal drift rate and the eccentricity vector are driven by perturbations which are dominant in the GEO region. These underlying perturbations are the tesseral acceleration due to the non-spherical potential of the Earth and the Solar Radiation Pressure (SRP) force.
The analysis of the longitudinal motion concerning active spacecrafts reveals a parabolic evolution that can be treated with two complementary approaches: a curve fitting using a simplified physical model and a Least Square (LS) fitting method. Afterwards, the manoeuvre is assumed to be at the intersection of two consecutive parabola previously identified.
The manoeuvre detection with the eccentricity vector relies on a more complex dynamical model. A semi-analytical orbit propagator, STELA [1], is used to obtain the expected evolution of the eccentricity vector. This evolution is then compared with the observed data from the Two-line elements (TLE) where a deviation marks the presence of a manoeuvre.
The detection performance has been assessed by comparing the results to historical test objects where the manoeuvre epochs are known in advance.

Keywords: manoeuvre detection; geostationary orbit; orbital perturbations; least-squares filters; Two-line elements; station keeping.

[1]STELA is available in `https://logiciels.cnes.fr/en/content/stela`

1. INTRODUCTION

The number of man-made space objects is dramatically growing nowadays. The continuous monitoring and studying of these objects are necessary to keep their number under control and ensure safe space operations. With respect thereto, international guidelines recommend decongesting the most populated space regions from satellites arriving at the end of their operational lifetime by performing post-mission disposal (PMD) strategies. Being able to assess the efficiency of PMD strategies is then essential to determine the guidelines compliance. For that it is required to detect when a satellite becomes inactive, that is to say, when it arrives to the end of its lifetime and it is no more under control. In general, a satellite is considered to be functional if it is still performing periodic manoeuvres to stay within the orbital operation configuration.
The analysis of existing catalogue for detecting manoeuvres has been studied in the last 15 years. [7] developed in 2008 a method to detect space events including orbit manoeuvres. The method processes state vector data associated with the catalogue of tracked objects. Sequential data are processed using a moving window to filter and estimate a parameter's value, for example, the semi-major axis for Low Earth Orbit (LEO) spacecrafts. Parameter dispersions are found by differencing its expected value and its actual value. When a deviation from its expected value exceeds a predefined threshold, an event is declared. The underlying idea of this method has been extensively used in future works. [6] presented two novel methods, the first one called TLE consistency check (TCC) and the second one called TLE time series analysis (TTSA). The TCC method detects events by comparing a published TLE data with a propagated state and analysing the spatial difference between the two. The TTSA method uses the time series of an object containing the orbital elements, or a derived quantity thereof, and evaluates it for any type of unexpected changes by methods from robust statistics and harmonic analysis. Although all these methods can be applied to any element set parameter or a derivative of one or more TLE parameters, they are usually applied to the semi-major axis to assess the behaviour of LEO spacecrafts. The performance when applied to other orbital parameters has not been still extensively assessed. The only work found by the au-

thors applied to a different orbital region is [3]. In that paper, signal processing techniques are applied on public domain TLE data to enhance the ability to detect orbital changes from the noise in raw TLE data. Once inconsistent outliers are filtered out, their work processes each orbit state with a temporal lead trail window of surrounding orbit states being propagated over a range of common epochs with key metrics being recorded. Two different methods of characterizing manoeuvres history are then implemented. The first method, Detection Method, uses metrics derived form comparison between adjacent orbit states in order to identify times where it is statistically probable that the satellite performed a manoeuvre. And, the second method or the Frequency Fit Method performs a manoeuvre frequency fit to the data in order to determine to what degree any pattern of periodic manoeuvring exists. The characterization function which is assessed in all this process is the maximum difference of radial, intrack, and cross-track magnitudes over one orbital period. The present paper presents a promising method to detect historical in-plane manoeuvres of satellites on a geostationary orbit (GEO). The novelty of this work is to introduce in the algorithm the particularities of the GEO dynamics such as the natural longitudinal drift. These considerations of the GEO orbital evolution allow us to select the most appropriate parameters to be assessed for the manoeuvre detection. Since a manoeuvre changes the orbital state of the spacecraft, its effect can be detected by comparing the observed data to a reference evolution. The reference model is represented in this case by the dynamical model STELA based on a semi-analytical theory[5]. The observed data is provided by the public American space object catalogue[9]. The Two-line element (TLE) database contains the orbital state of each tracked object, however, not all six orbital parameters are interesting to study in terms of in-plane manoeuvres. The evolution of the longitude and of the eccentricity vector is immediately affected by a manoeuvre that changes the shape or the size of an orbit. Within the longitude analysis, the manoeuvre epoch is estimated by focusing on the manoeuvre strategy. An operational spacecraft usually performs a manoeuvre as soon as the longitude motion threatens to violate the operational deadband. Consequently, the longitude evolution follows a parabolic motion.[8] Two polynomial curves of second degree are laid over the observations: the first curve is derived from a simplified dynamical model and the second curve is directly obtained through a Least Squares fitting method. The discrepancy between the LS and physical fitted parabolas gives an indication on the quality of the input data, the TLEs. The detected manoeuvre epoch must be companioned by a confidential parameter that denotes the time range around the estimated epoch in which the manoeuvre is expected to have happened. The manoeuvre interval is then forwarded to the eccentricity analysis where the manoeuvre epoch is estimated more precisely by studying the divergence between the observed and expected eccentricity vector evolution. The latter is propagated with STELA after having estimated the area-to-mass ratio that is needed in order to model the perturbation effects forces accurately (i.e. SRP) upon which the performance of the dynamical reference model strongly depends. As soon as the observed eccentricity vector deviates significantly from the expected evolution, the epoch and the velocity ΔV of the manoeuvre can be recovered, too.

2. EQUATIONS OF MOTION

Six quantities are needed in order to represent the dynamical state of any point object in space. An example is the representation through the position and velocity vector. By focusing on a specific orbit region, one can make use of the orbit's characteristics and find a more convenient way of representing orbital elements. It often makes more sense to describe geostationary objects using the so-called *synchronous* elements which are defined as a set of the following parameters:

$$[\lambda_m, D, e_x, e_y, i_x, i_y] = [\lambda_m, D, \boldsymbol{e}, \boldsymbol{i}]$$

where λ_m denotes the mean longitude of the spacecraft and D the mean longitude drift rate. The latter implies that λ_m is not constant over time but drifts due to a deviation of the semi-major axis a from the semi-major axis of the unperturbed GEO a_{GEO}. Throughout this work study, a vector is denoted by a bold letter and scalar values by non-bold variables. Hence, $\boldsymbol{e}$ and $\boldsymbol{i}$ indicate respectively the eccentricity and inclination vector. $\boldsymbol{e}$ represents a vector in the equatorial plane pointing towards the orbit's perigee with a magnitude of e while $\boldsymbol{i}$ is the projection on the equatorial plane of the orbital pole, the axis perpendicular to the orbital plane, its magnitude is i.

$$\boldsymbol{e} = \begin{pmatrix} e\sin(\Omega+\omega) \\ e\cos(\Omega+\omega) \end{pmatrix} \qquad \boldsymbol{i} = \begin{pmatrix} i\sin\Omega \\ -i\cos\Omega \end{pmatrix} \tag{1}$$

Soop [8] presents a detailed derivation of the linearised motion of a geostationary spacecraft using synchronous elements. The advantage of linearisation is that it gives a simplified mathematical expression for the motion by linearly adding the different effects on the orbit. Therefore, the motion with respect to Earth is considered to be small and the spacecraft ideally at rest on its geostationary orbit. If the duration of the thrust Δt is short ($\leq 1\,\mathrm{h}$) with respect to the orbital period, one can approximate the thrust as impulsive and add the velocity increment to the current state vector:

$$\Delta \boldsymbol{V} = \int_{t_b-\frac{\Delta t}{2}}^{t_b+\frac{\Delta t}{2}} \frac{\boldsymbol{F}}{m} dt \approx \frac{\boldsymbol{F}}{m}\Delta t \tag{2}$$

where t_b is the mid point time of the thrust. This means, if the state vector before the thrust has been $(\boldsymbol{r}, \boldsymbol{V})$ the next state vector after the thrust will be $(\boldsymbol{r}, \boldsymbol{V} + \Delta\boldsymbol{V})$. As a result, a manoeuvre thrust does not instantly affect the satellite's position but directly changes its velocity according to Eq.(2). The change in the velocity components in radial, tangential and orthogonal directions are respectively denoted as: $\Delta V_r, \Delta V_t, \Delta V_o$. Considering the status of a spacecraft at thrust time t_b, the linearised

equations of motion become:

$$\Delta r = -a_{GEO}\left(\frac{2}{3}\Delta D + \Delta e_x \cos s_b + \Delta e_y \sin s_b\right) = 0 \tag{3}$$

$$\Delta\lambda = \Delta\lambda_0 + \Delta D\,(s_b - s_0) + 2\Delta e_x \sin s_b - 2\Delta e_y \cos s_b = 0 \tag{4}$$

$$\Delta\theta = -\Delta i_x \cos s_b - \Delta i_y \sin s_b = 0 \tag{5}$$

$$\Delta V_r = V\,(\Delta e_x \sin s_b - \Delta e_y \cos s_b) \tag{6}$$

$$\Delta V_t = V\,(\Delta D + 2\Delta e_x \cos s_b + 2\Delta e_y \sin s_b) \tag{7}$$

$$\Delta V_o = V\,(\Delta i_x \sin s_b - \Delta i_y \cos s_b) \tag{8}$$

where s_b is the sidereal angle at thrusting time. $\Delta\theta$ expresses the change in the latitude that depends on the change in the inclination $\Delta\boldsymbol{i}$. The subscript "0" denotes all parameters at $t = t_0$. This linearisation is only justified for ΔVs less than $50\,\mathrm{m\,s^{-1}}$ when the thrust is much smaller than the orbital velocity ($V \simeq 3\,\mathrm{km\,s^{-1}}$). A detailed derivation of these equations is given by Soop [8]. An in-plane manoeuvre can either change the tangential, radial or both velocities. Accordingly, the orthogonal change can be neglected. In case of a tangential burn, Eq. (3)-(8) reveal the following solutions:

$$\Delta\lambda_0 = \frac{3\Delta V_t}{V}(s_b - s_0) \tag{9}$$

$$\Delta D = -\frac{3\Delta V_t}{V} \tag{10}$$

$$\Delta\boldsymbol{e} = \frac{2\Delta V_t}{V}\begin{bmatrix}\cos s_b \\ \sin s_b\end{bmatrix} \tag{11}$$

and in case of a radial change, the solutions are the following:

$$\Delta\lambda_0 = -\frac{2\Delta V_r}{V} \tag{12}$$

$$\Delta D = 0 \tag{13}$$

$$\Delta\boldsymbol{e} = \frac{\Delta V_r}{V}\begin{bmatrix}\sin s_b \\ -\cos s_b\end{bmatrix} \tag{14}$$

3. EFFECTS OF PERTURBATIONS

Station keeping (SK) thrusts are required because the spacecraft is subject to natural and unnatural perturbations but needs to maintain the desired orbit. There exists several natural sources of perturbations which have been summarised in Table 1. As shown, the dominant perturbations affecting the in-plane parameters are the tesseral terms of the non-spherical gravity field of Earth and the SRP.

Table 1. Overview of perturbations.

Perturbations	Effects
Non spherical gravity field of Earth	
– Tesseral terms	D
– Zonal terms	$\boldsymbol{i}$ (slightly), a
Three body system	$\boldsymbol{i}, \boldsymbol{e}$ (slightly)
Solar radiation pressure	$\boldsymbol{e}$

3.1. Non-spheric Earth potential

Earth's form does neither represent a sphere nor is its mass symmetrically distributed. In order to accurately model the Earth's gravity, its potential is expanded in a series. This study assumes that Earth's gravitational potential R is given by:

$$R = \frac{\mu}{r} + \mu\sum_{l=2}^{L}\sum_{m=0}^{l}\frac{R_e^l}{r^{l+1}}P_{lm}(\sin\theta)\cdot ... \\ ...\cdot(C_{lm}\cos m\lambda + S_{lm}\sin m\lambda) \tag{15}$$

where R_e is the radius of the Earth. The potential function is defined by a series development in spherical harmonics. P_{lm} denote the associated Legendre functions of degree l and order m. Considering the Earth as non-spherical introduces the angles θ and λ that denotes the spherical coordinates of the satellite. The C terms with $m = 0$ denote the zonal terms and represent the expansion that is rotationally symmetric caused by Earth's flatness. Hence the gravitational potential in this sense would be independent of λ. The tesseral terms, the terms where $m \geq 1$, introduce the gravitational potential as both latitude and longitude dependent caused by the unsymmetrical mass distribution of Earth's body. The tangential component of the gravitational acceleration due to the tesseral terms plays a major role with respect to the longitude drift. The disturbing acceleration is dominated by the coefficients with $l = m = 2$ and results in a potential given by:

$$R_{22} = \frac{\mu}{r}\left(\frac{R_e}{r}\right)^2 P_{22}(\sin\theta)\,(C_{22}\cos 2\lambda + S_{22}\sin 2\lambda) \\ = 3\cdot\frac{\mu}{r}\left(\frac{R_e}{r}\right)^2 J_{22}\cos^2\theta\cos\left[2\,(\lambda - \lambda_{22})\right] \tag{16}$$

where P_{22} denotes the associated Legendre function of second degree and second order. J_{22} and λ_{22} are terms combining the geopotential coefficients as:

$$J_{22} = \sqrt{C_{22}^2 + S_{22}^2} \tag{17}$$

$$\lambda_{22} = \frac{1}{2}\arctan\frac{S_{22}}{C_{22}} \tag{18}$$

Assuming that θ is approximately zero for GEO satellite, the acceleration in Eq.(16) becomes sinusoidally dependent on the longitudes with four nodes. The four nodes mark the longitudinal position at which the spacecraft does not encounter an acceleration and therefore, remains at rest. Two of them are so-called *stable* equilibrium points meaning that a spacecraft that is slightly dislocated from these nodes will experience a drift that brings it back to the stable points. That means that a GEO satellite at any longitude will accelerate towards the closest stable point and swings around this node like a pendulum. In contrast to this, the other two equilibrium points are known as *unstable* points. Unlike the stable nodes, the spacecraft would directly drift away in either direction, if it is not exactly located at the unstable points.The equilibrium points are located at the following longitudes:

- stable points: $75.1°$E and $105.3°$W
- unstable points: $11.5°$W and $161.9°$E

Due to the presence of these equilibrium points, the spacecraft drifts away from its mean longitude and the satellite's operator need to perform SK manoeuvres in order counteract the longitudinal acceleration caused by the tangential component of the tesseral gravitational attraction B:

$$\frac{d^2\lambda}{dt^2} = -\frac{3}{a_{GEO}}B \tag{19}$$

Considering, that B is constant within a small interval around the mean longitude, one can double integrate Eq.(19) and obtain the mean longitudinal motion. The evolution of the longitude follows a parabolic curve which is opened towards the direction of the nearest stable point [8]. The expression of the longitudinal acceleration is retrieved through the rate of change of the mean motion n set in relation to the Lagrange planetary equation. Recalling the model of the potential function up to $l = 3$ the longitudinal acceleration is given by:

$$\begin{aligned}\ddot{\lambda} &= -\frac{3}{a^2}\frac{\partial R}{\partial \lambda} \\ &= -3n^2\left\{-6J_{22}\left(\frac{R_e}{r}\right)^2 \sin 2\left(\lambda-\lambda_{22}\right)\right. \\ &\quad + \frac{3}{2}J_{31}\left(\frac{R_e}{r}\right)^3 \sin\left(\lambda-\lambda_{31}\right) \\ &\quad \left. - 45J_{33}\left(\frac{R_e}{r}\right)^3 \sin 3\left(\lambda-\lambda_{33}\right)\right\}\end{aligned} \tag{20}$$

where J_{lm} and λ_{lm} represent the notion for the combined harmonic functions of Earth gravity potential field [4].

$$J_{lm} = \sqrt{C_{lm}^2 + S_{lm}^2} \tag{21}$$

$$\lambda_{lm} = \frac{1}{m}\arctan\frac{S_{lm}}{C_{lm}} \tag{22}$$

3.2. Solar radiation pressure

Even though electromagnetic radiation is massless, it can still transfer momentum when it moves with speed of light and hits an object on its path. The exerted pressure is called *Solar Radiation Pressure* (SRP). The SRP generates a force on the spacecraft which is proportional to its cross-section S:

$$F = PS\left(1+\epsilon\right) \tag{23}$$

where ϵ is the surface reflectivity coefficient and P is the pressure exerted by the radiation on an orthogonal surface in the vicinity of the Earth ($P \simeq 4.56 \times 10^{-6} N/m^2$). The acceleration is always directed away from the Sun and depends on the area-to-mass ratio (S/m) and ϵ.

$$\frac{F}{m} = P\left(1+\epsilon\right)\frac{S}{m} \tag{24}$$

Since it is difficult to express the varying cross-section and reflectivity of a spacecraft, it is common to model the acceleration with one single parameter, the effective area-to-mass ratio defined as:

$$\sigma := \left(\frac{S}{M}\right)_{eff} = \frac{S\left(1+\epsilon\right)}{m} \tag{25}$$

The only orbital element which is affected by the SRP is $\boldsymbol{e}$ because the mean effect on a and i vanishes when averaged over one sidereal day. In the following, the mean evolution of the eccentricity vector encountered by SRP is derived.
It is assumed that the spacecraft is positioned at a sidereal angle s and the tangential and radial component of the velocity due to the radiation pressure differential dV are expressed as:

$$dV_t = \sin\left(s - s_\odot\right) dV \tag{26}$$

$$dV_r = -\cos\left(s - s_\odot\right) dV \tag{27}$$

with $s_\odot$ as the sidereal projection of the Sun on the orbital plane. Recalling the differential equation for the eccentricity vector $\boldsymbol{e}$:

$$\frac{d\boldsymbol{e}}{dt} = \frac{2}{V}\begin{bmatrix}\cos s \\ \sin s\end{bmatrix}\frac{dV_t}{dt} + \frac{1}{V}\begin{bmatrix}\sin s \\ -\cos s\end{bmatrix}\frac{dV_r}{dt} \tag{28}$$

By integrating Eq.(28) over one sidereal day, the mean drift rate of $\boldsymbol{e}$ is given by:

$$\frac{\delta \boldsymbol{e}}{\delta t} = \frac{3P\sigma}{2V}\begin{bmatrix}-\sin s_\odot \\ \cos s_\odot\end{bmatrix} \tag{29}$$

This shows that the mean drift goes in the direction +90° from the Sun and it changes throughout the years because of its varying sidereal angle of the Sun $s_\odot$ [8].

4. ALGORITHM DESCRIPTION

The present detection method takes as input parameters the historical data of a catalogue of Resident Space Objects (RSO). Within this work, the TLE catalogue provided publicly by the United States Air Force [9] have

been extensively used. Nevertheless, the method is not restricted to this particular database, and it can be used with any set of historical orbital data.
Before starting with the detection analysis, possible outliers in the TLE database need to be removed in order to keep the background information as reliable and accurate as possible. Afterwards, the manoeuvre detection starts by studying the longitudinal evolution. Therefore, two fitted curves are laid over the longitudinal data. The first curve is derived from the theoretical longitudinal acceleration of a spacecraft presented in the previous section, it will be useful to check the quality of the input data. The second curve is obtained by a LS order-2 polynomial fit over the longitude data points. This second curve is entirely based on the input data, and, for that reason, the intersections of consecutive LS parabolas are considered as an estimation of the manoeuvre epoch. The accuracy of the estimated manoeuvre epoch depends on the quality and quantity of the available TLEs. Consequently, it is convenient to label the estimated manoeuvre epoch with a confidential parameter that gives a time range around the estimation in which the true manoeuvre is expected to have been executed.
The analysis is then continued by further studying the eccentricity vector evolution. Therefore, the interval characterized by the confidential parameter is forwarded to the eccentricity detection algorithm that shall identify a more precise manoeuvre epoch through the comparison with the propagated evolution performed with STELA. The use of a more complex propagator than SGP4 is necessary to consider the effect of the SRP in the propagation. The choice of the semi-analytical propagator STELA over a numerical one is based on computational time considerations. Afterwards, the compatible in-plane $\Delta \boldsymbol{V}$ is characterized by derived from the change on the orbital parameters (see Eq. (9)-(14). Because the sampling of the TLE data hinders the recover of the actual number of burns and the size of each individual velocity change $\Delta \boldsymbol{V}_i$, the manoeuvre is considered as a single burn where the estimated $\Delta \boldsymbol{V}$ shall be equal to the effective velocity change due to all executed burns.
A schematic summary of the implementation is provided in Figure 1

4.1. Longitude analysis

In theory, geostationary spacecrafts remain fixed at the same sub-satellite point, if all perturbations have been neglected. However, in reality, the asymmetric Earth gravitational potential is the main disturbing acceleration that lets this point drift along the equator [1]. Therefore, satellite operators need to perform the so-called Station Keeping (SK) manoeuvres that allows the spacecraft to be maintained within a longitude window (deadband) and compensate the drift. As previously seen, the mean longitude motion describes a parabola function. Over time we retrieve a series of parabolas jointed by cusps at the moments when a SK manoeuvre has been performed.

4.1.1. Procedure to filter out outliers

The spacecraft's longitudinal motion is derived from the historical data. Hereby, all aberrant TLEs and data points which are epoch-wise closer than 12h to each other have been removed after running through several filters. The objectives of the filters are:

- Removing multiple TLEs found within one revolution,
- Removing large outliers which violate the deadband,
- Removing outliers by correcting the longitude evolution.

For the first objective, the algorithm loops through the entire time history and keeps only one TLE per revolution. Multiple longitudinal data within one day need to be removed since their presence could bias the processing done on the data set. Consequently, TLEs which are epoch-wisely too close to each other are removed through this method. Tests have shown that the first TLE is in general more reliable. Hence, in case of multiple TLEs separated by less than 12h, the first TLE is chosen for analysis.
In the second step, large outliers violating the deadband shall be removed. This filtering technique consists of two parts: In the first part, λ_m is set to the mean of the mean longitudes over the entire time history and the deadband half-width $\delta\lambda$ is initialized to $1\,\mathrm{deg}$. All data points which violate this initial deadband are considered to be aberrant and are removed from the time history. In case more than $30\,\%$ of the entire data set is removed, it is assumed that the object does not perform any SK manoeuvres and is drifting naturally, hence we consider that object as a debris. The selection of $\delta\lambda = 1\,\mathrm{deg}$ as initial half-width is reasonable because the typical values range from $0.1\,\mathrm{deg}$ to $1\,\mathrm{deg}$.[8]. In the second part, the current mean, minimal and maximal longitude over the entire time history are computed. $\delta\lambda$ is then defined in accordance to the current minimum and maximum in the longitude evolution as followed:

$$\delta\lambda_{min} = \lambda_m - \lambda_{min} \tag{30}$$
$$\delta\lambda_{max} = \lambda_{max} - \lambda_m \tag{31}$$
$$\delta\lambda = \min\left(\delta\lambda_{min}, \delta\lambda_{max}\right) \tag{32}$$

As Eq.(32) implies, the longitude extremum, that causes the larger half width deadband size, is considered as an outlier and will be removed from the time history. Repeating this step, while constantly updating λ_m, λ_{min} and λ_{max}, will eventually lead to:

$$|\delta\lambda_{max} - \delta\lambda_{min}| \leq \epsilon \tag{33}$$

where ϵ is empirically set to $5 \times 10^{-2}\,\mathrm{deg}$. Ideally, ϵ would have been zero, if λ_m had not been biased because of the sampling of the TLE data.
In the third step, aberrant values are removed from the time history while correcting the longitude evolution. In

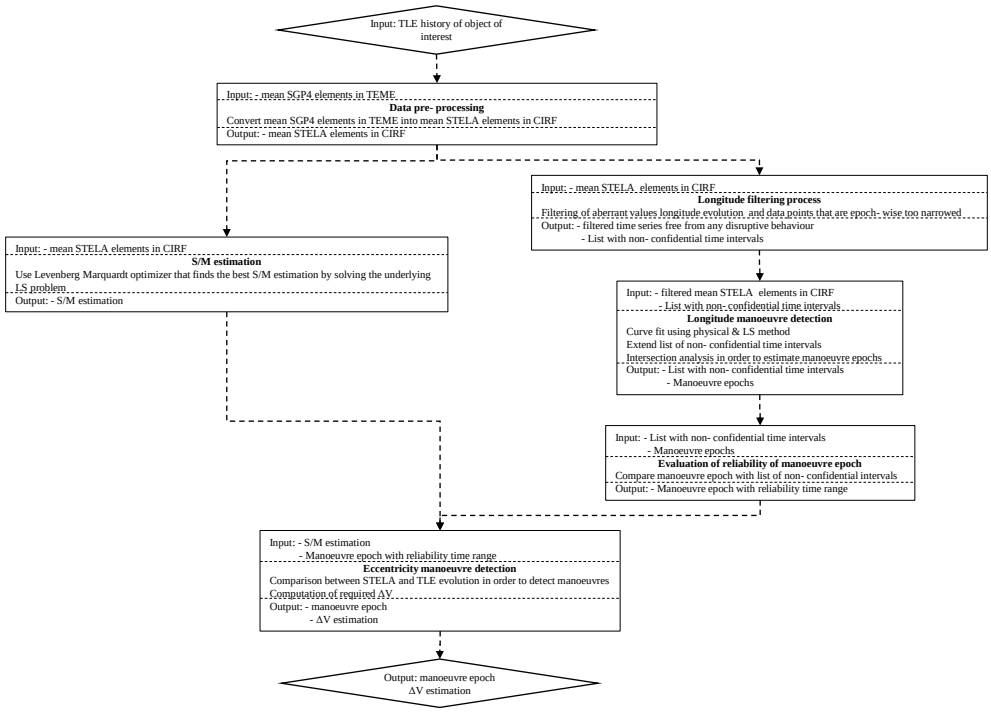

Figure 1. Algorithm scheme

principle an outlier is a local extremum but an extremum does not necessarily have to be an outlier. Instead, an extremum can also be a vertex point or a cusp due to a manoeuvre.

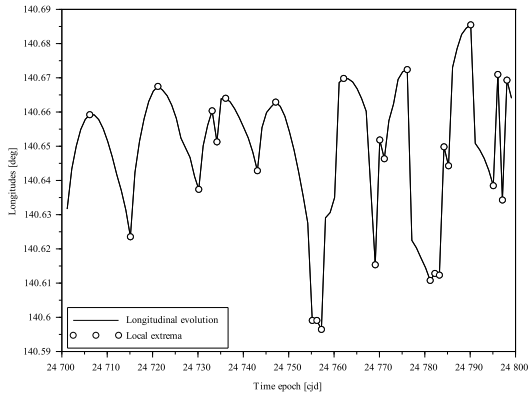

Figure 2. Longitude evolution [deg] of NORAD 40267 between 17/08/2017 and 25/11/2017 after having removed multiple TLEs within one revolution and large outliers from the time history. The dots mark the presence of a local extremum in the longitudinal evolution. Those extrema occur as bundles of different sizes: either they appear as an individual or as a sequence.

In the following, these kind of extrema are denoted as *true* extrema because these types do not disturb the behaviour of the parabola. Since the goal is to detect manoeuvres in the longitudinal evolution, it is necessary to differentiate between true extrema and the extrema due to outliers. Therefore, the algorithm iterates through the longitude history and extracts every local extremum. These extrema occur in so-called *bundles* which can vary in size as shown in Figure 2.

In contrast to bundles of size one whose extremum indeed indicate the presence of a true extremum, bundles of size $N > 1$ surely contain one or more outliers. Even though the latter disturb the parabolic trend of the longitudes, the trend can still be recovered, especially in the case of bundles of size two or three. In the following, these cases will be examined more in detailed:

i) Bundles with size two
As shown in Figure 3 there are only two scenarios in which these bundles can occur in the longitude evolution. By knowing the underlying trend, it is possible to recognize the outlier in the bundle by comparing the values of the bundle with its neighbours. For example, knowing that the trend is decreasing, the maximum in the bundle cannot be higher than the left neighbour and the minimum cannot be lower than the right neighbour and vice versa in case of a rising trend. In case this analysis has not yet revealed the outlier in the bundle, the algorithm propagates the state with STELA starting from the epoch of the left neighbour towards both extrema epochs

in the bundle. For the propagation, a precise estimation of the effective area-to-mass ratio is needed in order to achieve an accurate estimation for the final state of the satellite. The propagated longitudes are then compared with the observed data given by the TLEs.

$$\Delta E_1 = |\lambda_{prop,E_1} - \lambda_{E_1}| \tag{34}$$
$$\Delta E_2 = |\lambda_{prop,E_2} - \lambda_{E_2}| \tag{35}$$

ΔE_1 and ΔE_2 are the differences between the propagated longitude λ_{prop} retrieved from STELA and the longitude derived from the TLEs of the corresponding extrema E_1 and E_2 in the bundle. The extremum that generates the largest ΔE is considered as the outlier and will be removed from the time history. In case both extrema reveal a ΔE in the same range, both TLEs are considered as aberrant. In summary, this method will either remove both extrema in the bundle as outliers or only one of them and corrects the evolution of the parabola.

ii) Bundles with size three
There are two scenarios that yield the case of having exactly three extrema in a row. As can be seen in Figure 4 and Figure 5 the trend before and after the bundle is always reversed because the first and the last extremum are of the same type, either a maximum or minimum. Eventually, this leads to the conclusion that such bundles hide the presence of a true extremum. Knowing, that within the time interval of the bundle there must be a true extremum, will not help to eliminate the outlier but it will enable the recovery of the trend. For this purpose, one of the extrema needs to be removed from the time history and the algorithm always selects the middle one. The reason for this is it is certain that a new bundle of size three is not created as shown in Figure 5 but the algorithm ensures to have transformed the bundle into one of size one.

In the next step, the type of SK manoeuvre is computed. To recover the opening of the parabolas, it is necessary to compute the mean longitude over the entire time history. Moreover, it is significant to know which stable point is the closest one to the spacecraft to derive the direction towards it is accelerated. The direction of the opening of the parabola also gives the information about the type of the performed in-plane SK manoeuvre. An east manoeuvre is performed in case of a positive longitudinal acceleration and west SK burns are thrusted to counteract a negative longitudinal acceleration. Accordingly, if the range of the longitudes is generally defined from $0\,\mathrm{deg}$ to $360\,\mathrm{deg}$, one can see that upwardly opened parabolas correspond to east manoeuvres and vice versa for the case of west manoeuvres. From the type of manoeuvre and the opening of the parabolas, one can derive if either the maxima or the minima in the longitude evolution mark the extrema related to the manoeuvre. However, one should keep in mind that the current longitudinal evolution is still disrubted by bundles of size larger than three. These bundles hinder the fit of the parabolas over the data points. Even so, analysing the concrete size and position of these bundles in the longitude evolution leads to the following possibilities in order to handle their disruptive behaviour:

i In case the size of the time interval of the bundle is $< T$, where T is the mean duration between two manoeuvres, and the bundle hides a true manoeuvre extremum, then the intersection between the flanking parabolas are capable of recovering the true extrema. In Figure 6, the flanking parabolas are the second and the third parabola in the illustration. Consequently, the interval is removed before the parabola fitting of the longitudes. However, the recovered extremum by the intersection of the flanking parabolas (and the related manoeuvre epoch) is denoted as less reliable.

ii In case the size of the time interval of the bundle is $< T$ but the bundle does not hide a true manoeuvre extremum, as presented in Figure 7, the action will be the same as in the first case: the disruptive interval is removed following the fit of the parabolas.

iii This case creates the most problematic situation as seen in Figure 8. Due to the disruptive evolution of the TLEs, there is no way to analyse the manoeuvre history if the time interval is too long ($> T$).

4.1.2. Parabola fit

In this study, two techniques have been developed for the fit of a mathematical parabola equation over the observed data: the *physical* and the *Least squares* (LS) approaches. In both methods, a mathematical polynomial of second order is derived representing the longitudinal motion of the satellite over time. The spacecraft continues naturally to follow the parabola as long as there is no further acceleration that gets the satellite off course such as a manoeuvre thrust. The derivation of the parabola equations using the two different techniques shall be presented in the following:

i) Physical approach
The Earth's gravitational attraction can not be considered as symmetric and its mass concentrated in a point mass. Instead, the gravitational potential function given in Eq.(15) is used to model the potential of the spacecraft encountering the gravity field of the Earth. As given in Eq.(20), the tesseral terms of the gravitational potential of the Earth cause an acceleration of the satellite's mean longitude. Since the longitudinal deadband is usually very small, one considers the longitudinal acceleration as constant. Under this assumption, the solution for the longitude motion is derived as follows:

$$\lambda = \lambda_0 \mp \dot{\lambda}_0 (t - t_0) \pm \frac{1}{2}\ddot{\lambda} (t - t_0)^2 \tag{36}$$

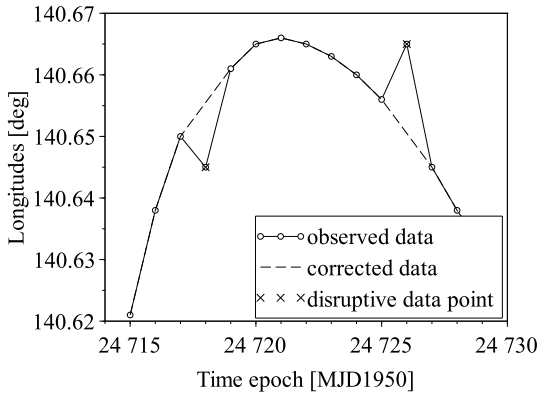

Figure 3. Example of a parabola with two bundles of size two. The outliers detected by the algorithm are marked in red. In the first case, STELA will recognize the underlying minimum as outlier while in the second case, the maximum directly reveals itself as aberrant because its longitude is larger than the one of the bundle's left neighbour.

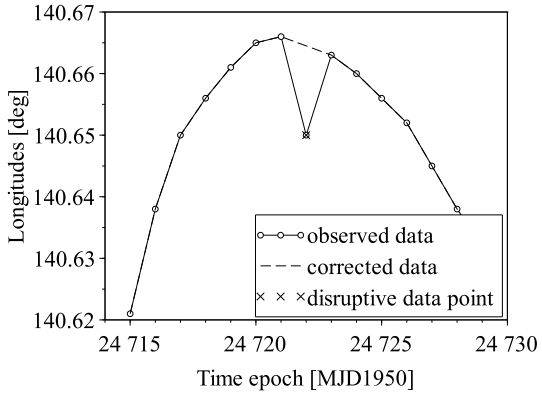

Figure 4. Example of a triple bundle at the vertex of the parabola.

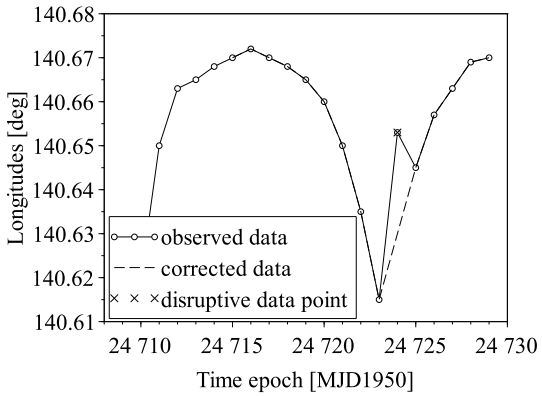

Figure 5. Example of a triple bundle that hides a true manoeuvre extremum.

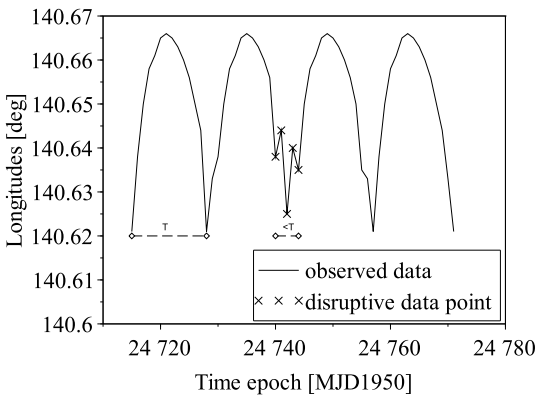

Figure 6. Example of a multi-extrema bundle that hides a true manoeuvre extremum.

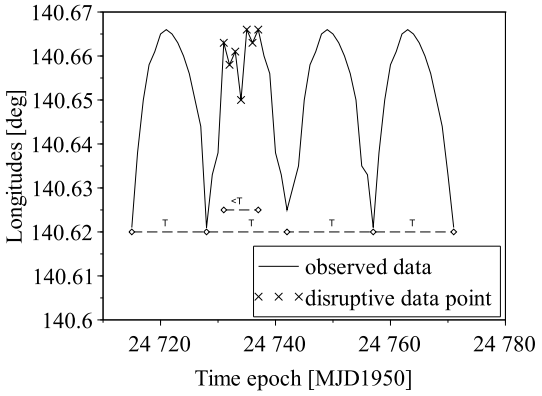

Figure 7. Example of a multi-extrema bundle that disrupts the evolution of a parabola

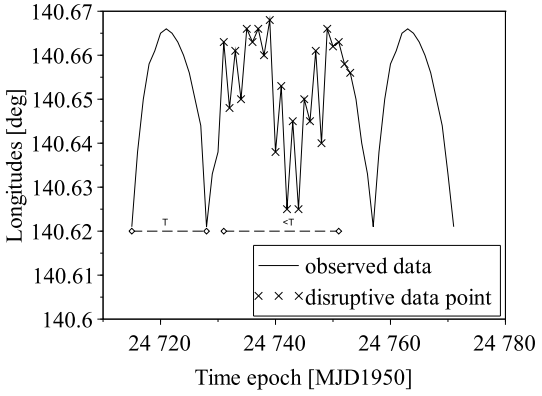

Figure 8. Example of a multi-extrema bundle that spans a time interval which is larger than T

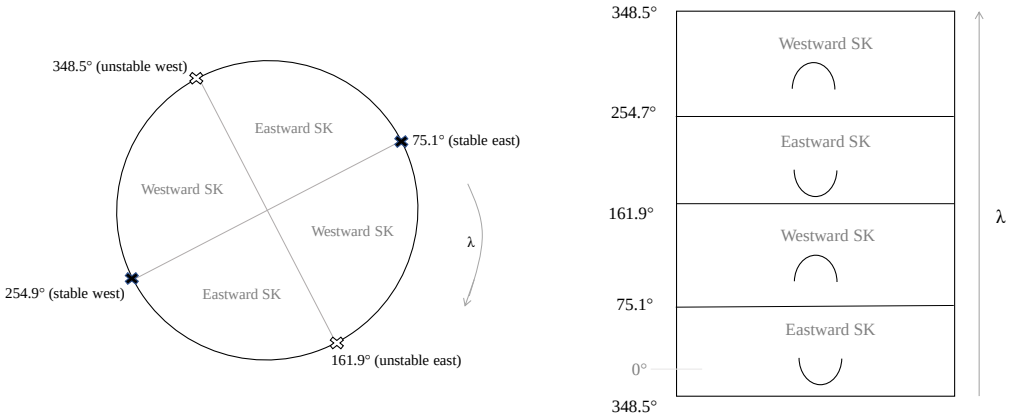

Figure 9. Relation between stability points and opening of parabola.

where "0" indicates the corresponding initial values at $t = t_0$:

$$\begin{aligned} \lambda_0 &= \lambda_m \pm \delta\lambda \\ \dot{\lambda_0} &= 2\sqrt{|\ddot{\lambda}| \cdot \delta\lambda} \end{aligned} \tag{37}$$

where $\ddot{\lambda}$ comes from Eq. (20) and $\delta\lambda$ and λ_m are derived in the previous analysis on the outliers filtering.
As mentioned above, depending on the opening of the parabolas, the signs of Eq.(36) change.[2] In order to have the parabola equation in the same format as for the LS fit, Eq.(36) is re-arranged into:

$$\lambda = a_p t^2 + b_p t + c_p \tag{38}$$

where:

$$\begin{aligned} a_p &= \pm\frac{1}{2}\ddot{\lambda} \\ b_p &= \mp\left(\dot{\lambda_0} + \ddot{\lambda} \cdot t_0\right) \\ c_p &= \pm\frac{1}{2}\ddot{\lambda} \cdot t_0^2 \pm \dot{\lambda_0} \cdot t_0 + \lambda_0 \end{aligned}$$

Here, the subscript "p" marks the coefficients derived with the physical method of fitting the parabolas.
The physical fit sets up an equation that does not take into account all forces that could potentially affect the longitudinal behaviour of the spacecraft, but considers only the effect of the main harmonics of Earth's potential on a perfect geostationary orbit. The fitted parabolas are then just representing a model which eventually reaches its limit in terms of accuracy, having an impact on the estimation of the manoeuvre epoch. In addition, it might occur, that some days before an east-west manoeuvre, a north-south manoeuvre has been performed that may disturb the longitudinal motion. For these reasons, it is reasonable to fit the data using a LS method, which is presented in the next step. This physical approach is however necessary to be able to determine if the LS fit is reliable enough. Indeed, the LS solution only takes into account the observed data (TLEs) and an potential poor quality of them could lead to inaccurate characterization of the manoeuver, situation that can be detected by comparing the results of both approaches.

ii) Least squares approach
The underlying principle aims to generate a curve of second degree that is laid over the data in such a way that the sum of the squared residuals resulting from the differences between the observed and the fitted data points on the curve are minimized. Adapted to the underlying problem, the goal is to find a ,b and c such that Π is minimized:

$$\Pi = \sum_{n=1}^{m} \left[y_n - \left(a\,T_n^2 + b\,T_n + c\right)\right]^2 \tag{39}$$

where m is the number of TLE data within the time history and y_n denotes the observed longitude derived from the TLEs. For the sake of better readability, the variable T_n is defined as:

$$T_n := (t_n - t_0)$$

The linear equation system is then given as:

$$M \cdot \begin{pmatrix} a \\ b \\ c \end{pmatrix} = \begin{pmatrix} \sum y_n \\ \sum T_n y_n \\ \sum T_n^2 y_n \end{pmatrix} \tag{40}$$

with:

$$M := \begin{bmatrix} \sum 1 & \sum T_n & \sum T_n^2 \\ \sum T_n & \sum T_n^2 & \sum T_n^3 \\ \sum T_n^2 & \sum T_n^3 & \sum T_n^4 \end{bmatrix}$$

where $\sum$ means the sum through all the TLE data $\sum_{n=0}^{m}$. In order to have the parabola equation in the same format as for the physical fit, the resulting parabola equation of Eq.(40) is re-arranged into:

$$\lambda = a_{LS}t^2 + b_{LS}t + c_{LS} \tag{41}$$

where:

$$\begin{aligned} a_{LS} &= a \\ b_{LS} &= b - 2c \cdot t_0 \\ c_{LS} &= a \cdot t_0^2 - b \cdot t_0 + c \end{aligned}$$

The subscript "LS" marks the coefficients of the parabola equation derived with the least squares method.

4.1.3. Confidential parameter

Throughout the manoeuvre analysis, all time intervals have been extracted which are assumed to be too disruptive to estimate the manoeuvre epoch accurately. The confidential parameter shall mark the estimated manoeuvre epoch as less reliable in case the parabola interval contains aberrant time series. There are three occasions within the algorithm at which the program evaluate the reliability of the data: during the search for aberrant parabolas, during the process when bundles of multiple extrema are removed and during the comparison of the physical and LS fit.
In the end, each manoeuvre epoch carries an attribute "reliable" in the form of a boolean. As a result, all the detected manoeuvre epochs which lie within the non-confidential time interval are treated as less reliable and the attribute is then set to false. Consequently, the manoeuvre epochs not affected by any abnormal TLE data reveal an accuracy within the range of one to two days. In contrast to this, detected manoeuvres within the non-confidential time interval usually deviate by several days from the true manoeuvre epochs.

4.1.4. Intersection analysis

As previously explained, the parabola fits using LS are preferred over the physical method and are therefore considered for the intersection analysis. The underlying principle is that the intersection between two consecutive parabolas reveals the estimated manoeuvre epoch. Assuming that the equations of parabola 1 and 2 are:

$$\begin{aligned} \lambda_1 &= a_1 t^2 + b_1 t + c_1 \\ \lambda_2 &= a_2 t^2 + b_2 t + c_2 \end{aligned}$$

then the zeros of the intersection equation are at:

$$\begin{aligned} t_{1,2} = &\pm \frac{\sqrt{(b_1 - b_2)^2 - 4\,(a_1 - a_2)\,(c_1 - c_2)}}{2\,(a_1 - a_2)} \\ &- \frac{(b_1 - b_2)}{2\,(a_1 - a_2)} \end{aligned} \tag{42}$$

In order to be considered as manoeuvre epoch, the related longitudes at t_1 or t_2 must lay within the longitude deadband. Finally, it is checked if the estimated manoeuvre epoch is contained within the non-confidential time intervals.

4.2. Eccentricity analysis

A single longitude manoeuvre cannot change the longitude without affecting the behaviour of the eccentricity vector. Consequently, it is advisable to couple the manoeuvre detection with the longitudinal and the eccentricity vector evolution. Up to now, the longitude manoeuvre detection is performed over the entire time interval of interest. The longitude algorithm returns a list of epochs of the estimated manoeuvres within this interval. The eccentricity manoeuvre detection is then only applied to each individual manoeuvre epoch in the list instead of to the entire time interval of interest. This means that, in the eccentricity analysis, a small interval around the manoeuvre epoch is studied to ensure that the smaller interval only contains one manoeuvre. In the following, these small intervals are referred to as *manoeuvre intervals*. Even though, the eccentricity analysis can be generalised and applied to the entire time history independently from the longitude strategy, this generalisation is not recommended since it would increase the risk of false positive detections. Therefore, in the current implementation, the eccentricity analysis is only applied to the manoeuvre intervals.
The principle of the eccentricity analysis relies on the prediction of the satellite's behaviour computed by an orbit propagator. Because $\boldsymbol{e}$ is mainly influenced by the effect of the SRP, a propagator containing in its dynamical model the SRP force is mandatory. This the reason of using STELA instead of SGP4. Furthermore, STELA propagation needs to take into account a well estimated value of the effective area-to-mass ratio σ that induces this perturbing effect. For that an orbit determaination is performed using the TLEs as observation data and considering the area-to-mass ratio as the only parameter to be estimated. This computation needs to be performed in an interval without manoeuvers where a natural evolution of the spacecraft is observed. Once σ is estimated, the algorithm will compare the observed $\boldsymbol{e}$ with the propagated state and assumes that a manoeuvre was performed in case the difference exceeds a certain threshold value. This threshold was empirically set to 1.3×10^{-5} and has been chosen by comparing the STELA propagation with the eccentricity vector evolution of several non-operational satellites which do not perform any manoeuvres. However, this threshold depends on the performance of the model and on the accuracy of the estimated

σ.
Before starting the eccentricity analysis, it must be ensured that the orbital parameters are converted from mean SGP4 elements to mean STELA elements. For the propagation process, the state of the spacecraft at each TLE epoch is propagated to the consecutive TLE epoch. Only at the first TLE epoch, the observed eccentricity vector is equal to the propagated state because a preceding TLE does not exist. Otherwise, at each epoch, the difference between the observation and the prediction by STELA can be computed. The dynamical model predicts the state of the spacecraft under the assumption that it only encounters natural perturbation forces. In reality, the satellite might perform manoeuvres which perturb the orbital state in addition but the thrusts are not taken into account by the dynamical model. Consequently, any large deviations between the dynamical model and the observed evolution indicates the presence of a manoeuvre. In the present analyses, $\boldsymbol{e}$ is split into its $x-$ and $y-$ component so that the differences are defined as:

$$\delta \boldsymbol{e_x} = \begin{pmatrix} e_{x,TLE_1} \\ e_{x,TLE_2} \\ \vdots \\ e_{x,TLE_k} \end{pmatrix} - \begin{pmatrix} e_{x,STELA_1} \\ e_{x,STELA_2} \\ \vdots \\ e_{x,STELA_k} \end{pmatrix} \tag{43}$$

$$\delta \boldsymbol{e_y} = \begin{pmatrix} e_{y,TLE_1} \\ e_{y,TLE_2} \\ \vdots \\ e_{y,TLE_k} \end{pmatrix} - \begin{pmatrix} e_{y,STELA_1} \\ e_{y,STELA_2} \\ \vdots \\ e_{y,STELA_k} \end{pmatrix} \tag{44}$$

where k is the number of TLEs in the time history. Afterwards, the algorithm iterates through $\delta \boldsymbol{e_x}$ and $\delta \boldsymbol{e_y}$ and sets all the entries to zero, in case the value lies below the threshold value. The velocity increment $\Delta \boldsymbol{V}$ caused by the manoeuvre can only be computed if the manoeuvre epoch is evident. Accordingly, the manoeuvre day must lay between the first TLE where the deviation between STELA and observation exceeds the threshold and the previous epoch. Furthermore, the algorithm is not capable of recovering the number of thrust nor the size of each individual $\Delta \boldsymbol{V_i}$ or the exact thrust time of each burn $t_{b,i}$. Instead, it is considered that the manoeuvre is performed as a single burn manoeuvre at epoch t_b and $\Delta \boldsymbol{V}$ is then derived from $\Delta \boldsymbol{e}$ that is defined as:

$$\Delta \boldsymbol{e}\left(\zeta\right) = \begin{bmatrix} e_{x,TLE}\left(\zeta\right) - e_{x,STELA}\left(\zeta\right) \\ e_{y,TLE}\left(\zeta\right) - e_{y,STELA}\left(\zeta\right) \end{bmatrix} \tag{45}$$

ζ marks the epoch at which the entries of $\delta \boldsymbol{e_x}$ and $\delta \boldsymbol{e_y}$ fall below the threshold value again, after the evolutions of the TLEs and STELA have deviated due to the manoeuvre. In contrast to the previously propagated values, $e_{x,STELA}\left(\zeta\right)$ and $e_{y,STELA}\left(\zeta\right)$ are not obtained by propagating the orbital state from epoch $\zeta - 1$ but from epoch α, where the entries of $\delta \boldsymbol{e_x}$ and $\delta \boldsymbol{e_y}$ were still below the threshold value before the manoeuvre took place. Hence, epoch α indicates the moment at which the manoeuvre has not yet affected the orbital state but is manifested one epoch later at $\alpha + 1$. Consequently, the right hand side of Eq.(45) shows the difference of the observed eccentricity vector after the manoeuvre and the expected value if the manoeuvre had not been performed. At this point it should be noted that in theory, that the deviation between the true state of the satellite and the prediction by the dynamical model is only non-zero at the instance of the manoeuvre. However, the analysis using TLEs reveals a peak behaviour with a certain width given by (α, ζ). This is related to the orbit determination process and the generation of TLEs which will be further discussed at a later point. Furthermore, it is assumed that the operator has intended to perform a pure longitudinal manoeuvre which means that the radial and orthogonal component of $\Delta \boldsymbol{V}$ are zero. Therefore, the subscript "t" in the velocity change can be left off while keeping in mind that $\Delta V = \Delta V_t$. The eccentricity change due to a tangential burn is given by Eq.(11). The corresponding ΔV results from the change of the numerical eccentricity:

$$\Delta V = \frac{|\Delta \boldsymbol{e}|\, V}{2} \tag{46}$$

where V is the velocity of the unperturbed geostationary spacecraft. Then, Eq.(11) can be rewritten as:

$$\Delta \boldsymbol{e} = |\Delta \boldsymbol{e}| \begin{bmatrix} \cos s_b \\ \sin s_b \end{bmatrix} \tag{47}$$

Due to the symmetry of the trigonometrical functions sine and cosine, it is not sufficient to only solve the equation in one component but the solution s_b must solve both terms in Eq.(47). The resulting s_b gives the angular position of the spacecraft on the orbital plane at the moment of the burn with respect to the $\boldsymbol{X}$- axis. That means, that s_b represents the fraction of the day at which the burn was fired. The exact manoeuvre hour of the day t_b is then retrieved by means of any reference point on the orbit where the epoch and the sidereal angle are known. Here, the epoch of this reference point is denoted as t_{ref} and its sidereal angle as s_{ref}. The manoeuvre hour is given by:

$$t_b = t_{ref} - \frac{12}{\pi} \cdot \left(s_{ref} - s_b\right) \tag{48}$$

The day of the manoeuvre lies between the TLE epoch where $\delta \boldsymbol{e_x}$ and $\delta \boldsymbol{e_y}$ have not exceed the threshold and its consecutive epoch day.

5. RESULTS

In the following, the performance of the detection methods using the longitudinal motion and the behaviour of the eccentricity vector shall be separately analysed from each other. Therefore, the detected epochs given by both methods are to be compared with the manoeuvre records of reference objects that are known in advance. The list of these reference objects was generated by the Space Debris modelling and risk assessment office of CNES. The testing of the longitude method included four satellites (NORAD ID: 23839, 24674, 25153, 40267) with a total number of 204 manoeuvres according to the manoeuvre history while only three satellites (NORAD ID:

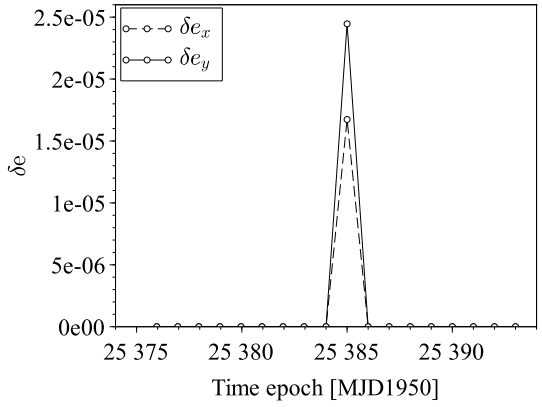

Figure 10. Difference in the x- and y-component of $\mathbf{e}$ *between TLE observation and STELA propagation at each epoch.*

Table 2. Manoeuvre detection results of NORAD 24671 in 2019. Epochs are given as day of the month.

Month	Manoeuvre history	Longitude analysis	Eccentricity analysis
Jan.	(16, 17)	18	
Feb.	6, (26, 27)	6, 25	7, 27
Mar.	18	19	19
Apr.	5, 24	4, 25	6, 26
May	15	17	17
Jun.	7	8	8
Jul.	1, 17	1, 18	2, 18
Aug.	7, 14, 23, 28	6, 23	8, 24
Sep.	(15, 16)	13	16
Oct.	9, 30	6, 31	11
Nov.	20	22	1, 22
Dec.	11	11	13

23839, 24674, 28912) with a total number of 68 manoeuvres were involved in the testing of the eccentricity vector method. As can be seen, not necessarily the same satellites were tested to evaluate the performance of both algorithms but they have been selected based on the manoeuvre strategy and the principle of the detection method. Both algorithms are only capable of detecting the manoeuvre as a whole but do not return the number of burns. However, different from the longitudinal method, the analysis of the eccentricity vector does not only give an estimation on the manoeuvre day but also on the position of the spacecraft on its orbit, from which the exact manoeuvre epoch time can be derived. Consequently, only satellites performing single burn manoeuvre have been used to evaluated the performance of the detection method using the eccentricity vector. Satellites performing two thrust manoeuvres separated by half a period can also be used for the performance analysis of the longitudinal method but are not suitable for the other.
Table 2 shows the results of both algorithms in detail for the case of satellite 24671 compared to its manoeuvre history. The manoeuvre epoch is given by the day of the month in 2019. Due to small number of TLEs, manoeuvres which were separated by only one sidereal day can generally not be detected as multiple manoeuvres but result in one manoeuvre estimation. These scenarios have been indicated with brackets as seen in the second column. The results show two false negative detections with the longitude analysis appearing in August 2019. On the other hand, the eccentricity analysis reveals three false positive detection that occur in January and August.

The statistical detection results of the longitudinal method are summarised in Table 3. The total number of true manoeuvres given by the operator records is 204 of which $93\,\%$ were correctly detected. A detection is considered to be correct if the interval described by the confidential parameter truly includes the actual manoeuvre epoch. However, in four cases, the algorithm managed to detect the manoeuvre but they where denoted with the wrong confidential parameter. Consequently, the manoeuvre records laid outside the estimated time range in which the manoeuvre were expected to take place. False detection can be either of an error type I, a false positive detection or of an error type II, a false negative detection. The tests resulted in nine false positive detection where eight of these estimated manoeuvre epochs were denoted as non confidential. As the table suggests, most of the false positive hits are due to satellite 40267. In general, the algorithm is prone to false positive detections in case the longitudinal evolution contains aberrant parabolas. Aberrant parabolas do not originate from the SK cycle but from the quality of the historical TLE series. TLEs are generated by a numerical fit of the orbit over discrete measurements of the spacecraft's state over a certain time interval. Aberrant parabola may occur in the longitudinal evolution if the orbit determination process reveals unstable results. Figure 11 shows the longitudinal motion of this satellite over several months after the start of the operational phase. The quality of the TLE data yields a disruptive behaviour of the longitudinal motion over which several short-term parabolas are fitted. These parabolas are considered as aberrant and reveal false positive detections.
In contrast to this, the testing revealed eleven false negative detection mainly occurring due to the TLE quality of satellite 23839. Aberrant data might not only result in extra short-term parabola but can appear as a bundle of multiple extrema that has been removed from the time series. The algorithm will not be able to recover a manoeuvre epoch, in case this bundle contained the presence of a true manoeuvre extremum. Instead the current parabola of the removed bundle is combined with the neighbour as seen in Figure 12 and Figure 13. Table 4 summarises the statistical analysis of the detection method with the eccentricity vector. As previously mentioned, the evaluation rather focuses on the correct estimation of the manoeuvre epoch time but not on the date. Also for this

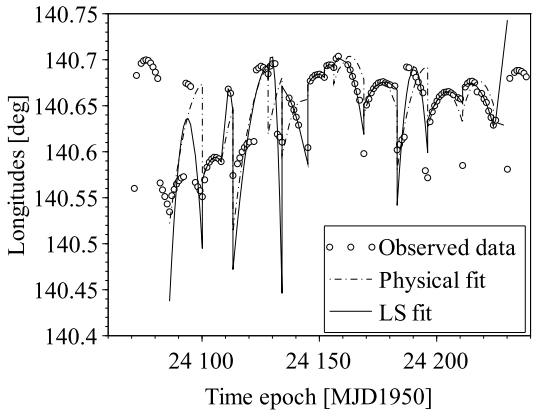

Figure 11. Disruptive longitude evolution [deg] of NORAD 40267 between 25/11/2015 and 14/05/2016.

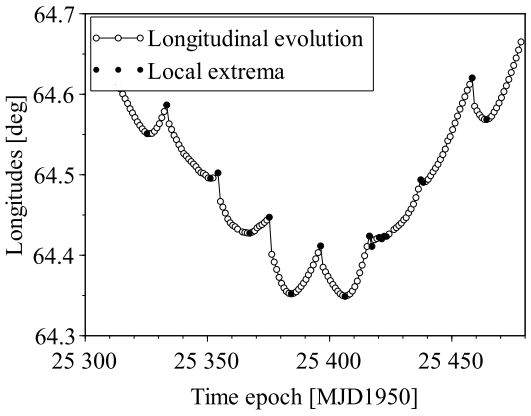

Figure 12. Longitude evolution [deg] of NORAD 23839 between 19/04/2015 and 04/10/2016 before having removed bundles of multiple extrema.

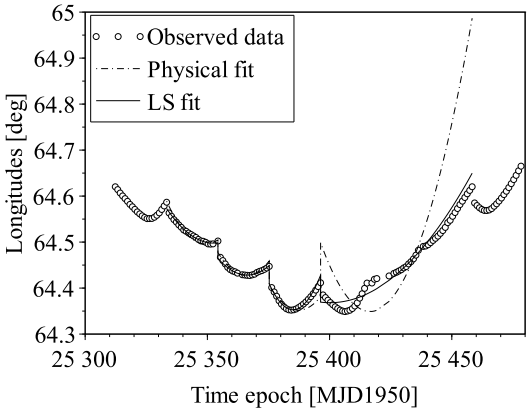

Figure 13. Longitude evolution [deg] of NORAD 23839 between 19/04/2015 and 04/10/2016. The multiple extrema bundle has been removed which, in this case, results in false negative detections.

performance analysis, the detected results were compared with the operational history. In case the estimation deviates by less than one hour from the true manoeuvre time, the prediction is considered to be very accurate, a deviation up to two hours is considered as accurate estimation and a large deviation counts as an inaccurate detection. Out of 68 manoeuvres, $68\,\%$ delivered at least a good estimation of the epoch time. In four cases, the method was not capable of detecting the underlying manoeuvres. The reason for this is that $\delta \boldsymbol{e_x}$ and $\delta \boldsymbol{e_y}$ defined by Eq.(43) and Eq.(44) show more than one peak. Hence, due to the quality of the TLE data, the manoeuvre epoch can not clearly be recovered. One would think that aberrant values have been already removed after the filtering process in the longitude analysis. However, there the data were filtered in order to recover the longitudinal trend. It might happen that the algorithm does not recognize a data point as aberrant because its longitudinal value is still compliant with the trend of a parabola. Hence, the value does not represent a problem in the longitudinal analysis but it might show as aberrant for the eccentricity analysis. Furthermore, the performance of this detection method strongly depends on the orbit determination process that generates the TLEs and the deviation between the true state of the spacecraft and the observed state given by the TLE data. The testing revealed an inaccurate estimation of the manoeuvre time in 18 cases. A possible explanation might be the width and the height of the peaks $\delta \boldsymbol{e_x}$ and $\delta \boldsymbol{e_y}$. One might think that a manoeuvre instantaneously changes the behaviour of the orbital parameter and consequently, the peaks of $\delta \boldsymbol{e_x}$ and $\delta \boldsymbol{e_y}$ must be very narrow. In theory, the deviation between the true state of the satellite and the prediction by the dynamical model is non-zero only at the instance of the manoeuvre. However, TLEs do not necessarily represent the true state, especially in case a manoeuvre was performed. When a satellite has manoeuvred, the orbit determination process might generate the corresponding TLE from an interval that takes into account discrete measurements before and after this manoeuvre. The set of observations is applied to statistical estimation techniques in order to derive a fitted orbit. As a result, the final orbit solution depends on the number of measurements and the accuracy of the perturbation model describing the dynamical environment.[10] However, a manoeuvre additionally affects the orbital state and the final orbit estimation becomes less accurate. This does not only have an impact on the height of $\delta \boldsymbol{e_x}$ and $\delta \boldsymbol{e_y}$ at the moment of the manoeuvre but generates a peak with a certain width as described in subsection 4.2. The width of the peak depends on the duration it takes until the determined orbit recovers from the manoeuvre. This point is reached when the interval of the orbit determination only takes into account measurements of the orbital state after the manoeuvre took place. That says the larger the width, the more time has passed since the true manoeuvre epoch. This has an effect on the computation of the Δe that is defined as the change

in the eccentricity vector due to a single burn manoeuvre. If a long time passes since the manoeuvring, Δe will additionally be affected by natural perturbations. Hence, recovering the effect only due to the manoeuvre is difficult and the resulting estimation of the manoeuvre hour is less accurate.

6. CONCLUSION

In the scope of this work, two techniques have been developed to detect in-plane manoeuvres from historical orbit data of geostationary satellites. The first method focuses on the longitude evolution and aims to recover the station keeping cycle by fitting the parabolic evolution of the longitude data and analysing their intersection. The method reaches its limit if the station keeping cycle is too short or if the sampling of the TLEs is to small to optimally fit the parabola evolution. The method might be extended by the analysis of the harmonics in the time series as it is presented by Lemmens and Krag[6] in order to reduce the number of false negative detection due to short manoeuvre cycles. The second method analyses the behaviour of the eccentricity vector and compares the observed evolution with the expected state predicted by the dynamical propagation model STELA. A manoeuvre is detected as soon as the derivation between both evolution exceeds a certain threshold value. The performance strongly depends on the performance of the dynamical model because it models the natural perturbation forces acting on the satellite. Among those forces, the solar radiation pressure is the dominant term that affects the eccentricity vector evolution. This perturbing effect, however, is induced by the spacecraft's effective area-to-mass ratio, hence, the modelling of the solar radiation pressure acceleration depends on an accurate estimation of this physical parameter. Furthermore, the tests have revealed that inaccurate detection estimation might originate from the orbit determination process perturbed from the manoeuvre incident itself.
In general, the ability to recover the manoeuvre history of satellites is important to analyse the life time of a satellite. In particular, it is of huge interest to know if a satellite has already reached its end of life and if its last manoeuvre has been performed in compliance to the IADC mitigation guidelines.

REFERENCES

[1] Peter Berlin. *The geostationary applications satellite*. 2. Cambridge University Press, 1988.

[2] Stoian Borissov, Yunhe Wu, and Daniele Mortari. "East–West GEO Satellite Station-Keeping with Degraded Thruster Response". In: *Aerospace* 2.4 (2015), pp. 581–601.

[3] Jacob Decoto and Patrick Loerch. "Technique for GEO RSO Station Keeping Characterization and Maneuver Detection". In: *Proceedings of the Advanced Maui Optical and Space Surveillance Technologies Conference,(AMOS)*. 2015.

[4] Heiner Klinkrad. "Space debris". In: *Encyclopedia of Aerospace Engineering* (2010).

[5] C Le Fèvre et al. "Compliance of disposal orbits with the French space operations act: the good practices and the STELA tool". In: *Acta Astronautica* 94.1 (2014), pp. 234–245.

[6] Stijn Lemmens and Holger Krag. "Two-line-elements-based maneuver detection methods for satellites in low earth orbit". In: *Journal of Guidance, Control, and Dynamics* 37.3 (2014), pp. 860–868.

[7] R.P Patera. "Space Event Detection Method". In: *Journal of Spacecraft and Rocket* 45.3 (2008), pp. 554–559.

[8] Erik Mattias Soop. *Handbook of geostationary orbits*. Vol. 3. Springer Science & Business Media, 1994.

[9] *Space-Track*. `https://www.space-track.org`.

[10] Jerome R Vetter. "Fifty years of orbit determination". In: *Johns Hopkins APL technical digest* 27.3 (2007), p. 239.

Table 3. Summary of manoeuvre detection by analysing the longitudinal motion.

Sat No	Time span	Number of manoeuvres (history)	Correct detections	Wrong confidential parameter	Error Type I	Error Type II	Total detections
23839	19/07/2018 to 28/02/2020	29	20	2	1	7	23
24674	11/07/2018 to 13/02/2020	31	29	-	-	2	29
25153	11/07/2018 to 30/01/2020	28	28	-	-	-	28
40267	09/07/2015 to 06/12/2019	116	112	2	8	2	122
Total		**204**	**189**	**4**	**9**	**11**	**202**

Table 4. Summary of manoeuvre detection by analysing the eccentricity vector motion.

Sat No	Time span	Number of manoeuvres (history)	Very accurate estimations	Accurate estimations	Inaccurate estimations	Error Type II	Total detections
23839	19/07/2018 to 28/02/2020	29	16	5	7	1	28
24674	11/07/2018 to 13/02/2020	31	12	8	8	3	28
28912	26/09/2018 to 05/02/2020	8	4	1	3	-	8
Total		**68**	**32**	**14**	**18**	**4**	**64**